Stress Concentration on PDMS: An evaluation of three numerical constitutive models using digital image correlation

Flaminio Cesar Sales [a], Andrews Souza [b,c,e], Fallconny R.S. Oliveira [a], Rui A. Lima [b,d], João Ribeiro [a,e,*]

[a] ESTiG, Instituto Politécnico de Bragança, 5300-252, Bragança, Portugal
[b] MEtRICs, Mechanical Engineering Department, Campus de Azurém, University of Minho, 4800-058, Guimarães, Portugal
[c] CMEMS, Minho University, Guimarães, Portugal
[d] CEFT, Faculdade de Engenharia da Universidade do Porto (FEUP), Rua Roberto Frias, 4200-465, Porto, Portugal
[e] CIMO, Instituto Politécnico de Bragança, 5300-252, Bragança, Portugal

ARTICLE INFO

ABSTRACT

The examination of hyperelastic materials' behavior, such as polydimethylsiloxane (PDMS), is crucial for applications in areas as biomedicine and electronics. However, the limitations of hyperelastic models for specific stress scenarios, with stress concentration, are not well explored on the literature. To address this, firstly, three constitutive models were evaluated (Neo-Hookean, Mooney-Rivlin, and Ogden) using numerical simulations and Digital Image Correlation (DIC) analysis during a uniaxial tensile test. The samples were made of PDMS with stress concentration geometries (center holes, shoulder fillets, and edge notches). Results of ANOVA analysis showed that any of the three models can be chosen for numerical analysis of PDMS since no significant differences in suitability were found. Finally, the Ogen model was chosen to obtain the stress concentration factors for these geometries, a property which characterize how discontinuities change the maximum stress supported by an element. Our study provides new values for variables needed to analyze and design hyperelastic elements and produce a foundation for understanding PDMS stress-strain behavior.

1. Introduction

The relevance of polymers and elastomers with high-performance properties, such as thermal and chemical stability, is well known, as they play a crucial role in the development of various applications, including aerospace, structural, biomedical, micro and nano technologies (Wolf et al., 2018). One of the most prominent elastomers in the biomedical and electronic fields is polydimethylsiloxane (PDMS) (Ariati et al., 2021). It is a biocompatible silicone (Montazerian et al., 2019)–(Souza et al., 2020) and has several desirable characteristics, for example, its high flexibility (Shi et al., 2020), (An et al., 2017), hydrophobicity (Wang et al., 2019), optically transparency (Sales et al., 2021). In biomedical fields, PDMS is utilized in microfluidic devices and microelectromechanical systems, enabling the development of devices for drug delivery, DNA sequencing, lab-on-a-chip manufacturing, and facilitating cell culture, disease analysis, and clinical diagnostics. PDMS plays a pivotal role in optical systems and is essential for wearable sensors. Furthermore, PDMS's biocompatibility extends to the fabrication or coating of medical implants, catheters, and pacemakers, thanks to its attributes such as low manufacturing cost, gas permeability, transparency, and low toxicity. Also, it has excellent resistance to biodegradation, chemical stability, good mechanical properties and ease of manufacture (Zhou et al., 2010)– (Miranda et al., 2021).

To understand the behavior of these polymers, many constitutive models were developed based on strain energy density functions. However, when analyzing materials that are able to face large strains, linear elastic assumptions are not valid and their behavior should be characterized using hyperelastic models, also called Green elastic models (Chang and Li, 2010). These models are a generalization of the linear elasticity and allow the analysis of large non-linear deformations of real-world scenarios, faced by most of the biological tissues, silicone parts and structures (Khaniki et al., 2023).

Several models were created as research about rubber-like materials advanced. Ronald Rivlin and Melvin Mooney's initial models, from the
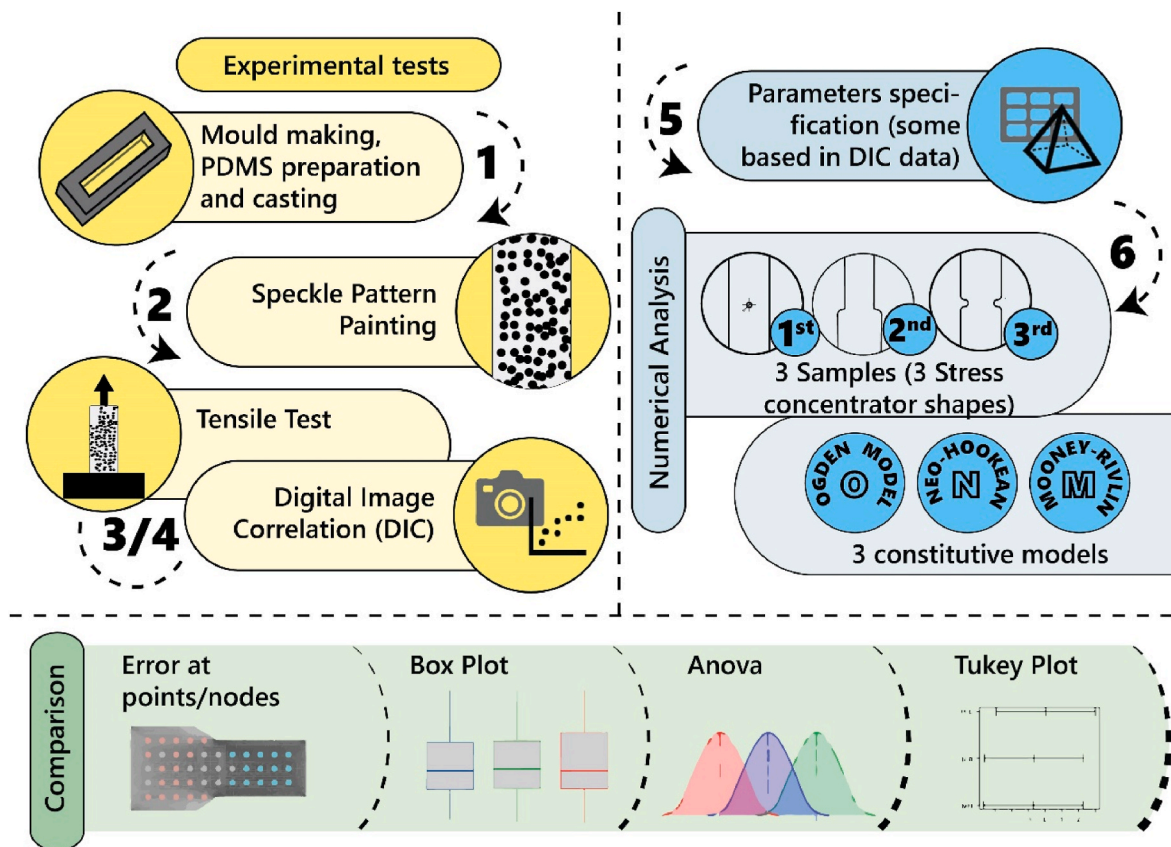

Fig. 1. Summary of the methodology: from the experimental tests to the numerical and static analysis.

1950s, were dependent on strain invariants and based on stress-strain responses measured empirically, (Rivlin, 1948). They were the Neo-Hookean and Mooney–Rivlin models. Later, other models emerged, such as the Ogden Model, which was dependent on the principal stretches (Ogden, 1972a).

For rectangular, or plane, elastomeric PDMS samples with thicknesses between 150 μm and 250 μm, studies in monotonic and cyclical loading conditions pointed the Ogden model as the best suit to simulate films over the entire uniaxial tensile test range (Song et al., 2022). Even so, at smaller strains, most models can mimic the hyperelastic behavior with minimal differences (Song et al., 2022). Studies using Ogden model have obtained more satisfactory results, both for uniaxial and axial tests when compared to others. However, this model may have limitations in some specific stress scenarios, which other models, such as the Mooney-Rivlin, may have better results (Kim et al., 2012). Additionally, there is a lack of research comparing these models in particular scenarios, such as those that involve stress concentration factors (SCFs).

Stress concentration factors (SCFs) play a pivotal role in comprehending and predicting the behavior of mechanical structures. They have been obtained through numerical simulations in various studies, which involve design features like holes, shoulders, and grooves. These features can lead to localized stress and strain distributions, potentially exceeding critical levels and causing structural failures. The accurate determination of SCFs, whether through analytical, computational (such as finite element analysis), or experimental methods, is crucial for assessing structural integrity and ensuring the long-term reliability of engineering components (Fukahori and Seki, 1993)– (Khajehsaeid et al., 2016). Despite some well-explored aspects, such as stress concentration around the center hole, most studies primarily rely on numerical simulations, with experimental approaches primarily limited to material parameter determination. Furthermore, there is a noticeable gap in research concerning stress concentration factors in

polydimethylsiloxane (PDMS), especially when considering fillets and edge notches.

One approach to carry out the comparison between the results obtained at the numerical simulations and experimental tests is by using Digital Image Correlation (DIC). DIC is a non-contact technique for measuring object's strain and deformation using a camera and software during a mechanical test (Rodrigues et al., 2016). It is ideal to analyze hyperelastic materials by comparing images of the object in its undeformed and deformed states over time (Ribeiro et al., 2019), (Sales et al., 2022). To ensure accurate measurements, a high-contrast unique pattern must be applied on the object's surface to avoid the correspondence problem (Song et al., 2022; Kim et al., 2012; Fukahori and Seki, 1993; Yang et al., 2008). This technique has been used in recent years in different methodologies to characterize the mechanical behavior of different materials (Pereira et al., 2020)– (Nunes, 2011a). In hyperelastic materials, such as PDMS, DIC proved to be adequate as it allows measurement of the complete material deformation field (Sales et al., 2022). Nunes et al. (Nunes, 2011b) successfully used an experimental approach based on the DIC method to investigate the mechanical behavior of PDMS through simple shear tests and estimated the angular distortions associated with different applied forces. J. Russ et al. (2020) employed DIC to study 3D printed polymeric composites subjected to large strains and compared qualitative and quantitative characteristics with numerical modeling. The work by K. K. Dwivedi et al. (2022) applied DIC to compare hyperelastic models and determined which model captured the mechanical behavior more accurately.

Deformation analysis along multiple points of the specimen via DIC enables a more accurate strain evaluation, especially when stress concentration factors are present (Russ et al., 2020). While many charts detailing these factors can be found in literature for metals, they are dependent on the shape of the structure and its main dimensions (Pilkey, 2020). However, one of the most explored fields is the evaluation of the
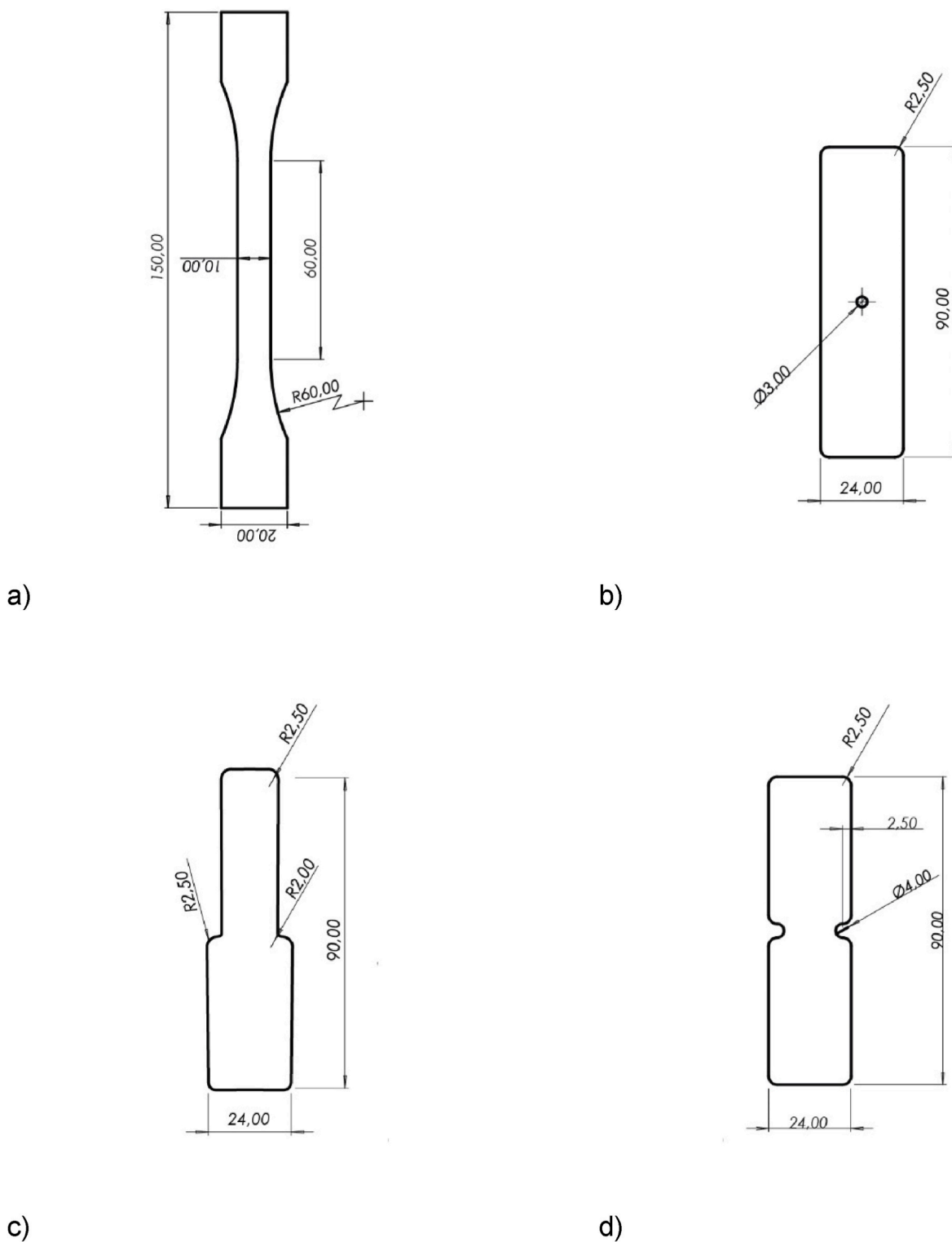
Fig. 2. Samples for both experimental and numerical analysis: a) Standard BS 2782 sample, 4 mm in thickness; samples with stress concentrators and 3 mm in thickness: b) with a central hole: c) shoulder-filleted: d) edge-nodded.

concentration factors in elastomers, but related to fiber reinforcement effects, not geometric characteristics (Khajehsaeid et al., 2016), (Khajehsaeid et al., 2016), (Myneni et al., 2021). Consequently, the impact of geometries, like holes, on the behavior of PDMS and other hyperelastic materials remains understudied.

In the work reported here, numerical analysis using three of the most known constitutive models for hyperelastic materials (Neo-Hookean,

Mooney-Rivlin, and Ogden) where compared with the digital image correlation obtained in uniaxial tensile tests of PDMS, one of the most distinguished hyperelastic examples. The samples had different shapes: regular dumbbell without stress raises and three others, which had different stress concentration geometries: a center hole, shoulder fillets, and edge notches. Thus, this allowed: (1) to verify which one of the previously mentioned constitutive models is more suitable for the
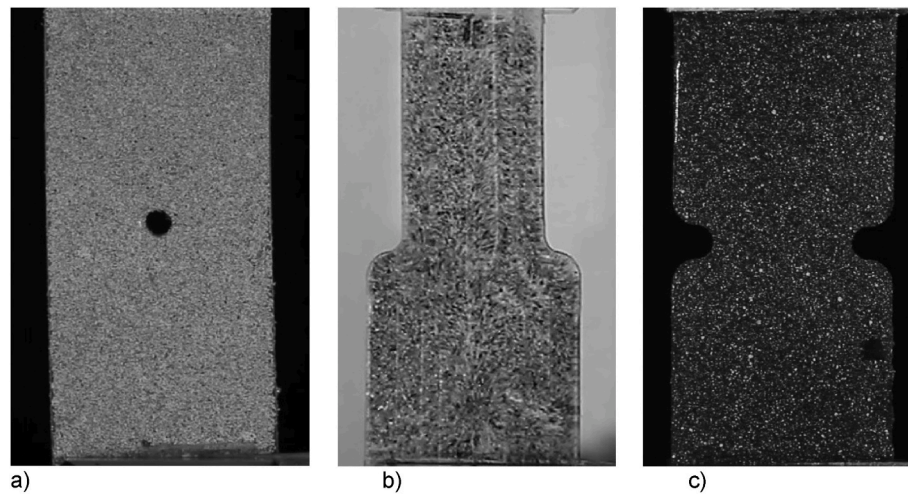
Fig. 3. Samples painted with speckle pattern: a) 1st sample, black pattern on white background; 2nd sample, black pattern on transparent background; 3rd white speckle on black background.
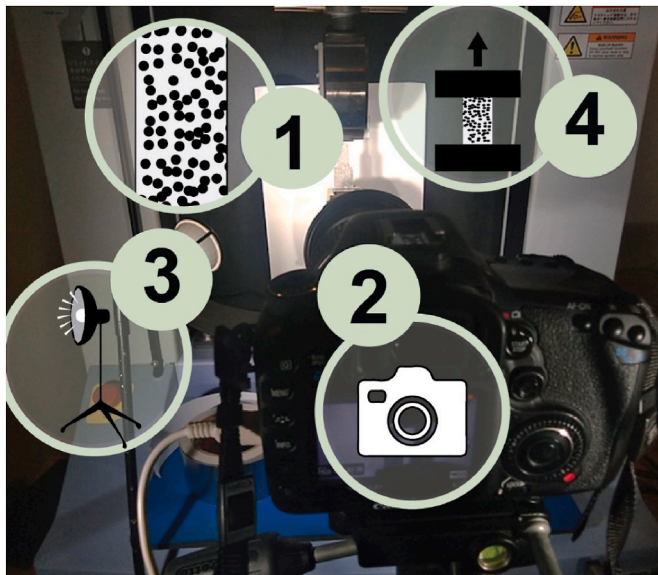

Fig. 4. Image acquisition system during the tensile test, indicating: 1 - Specimen; 2 - Camera; 3 - Lightning System; 4 - Universal Test Machine.

analyzed geometries and material; (2) to obtain the stress concentration factors for the three shaped inclusions mentioned.

2. Methodology

Fig. 1 is a summary of the entire methodology process. First, experimental tests were carried out, either to specify parameters needed in the analysis or to establish a comparison basis. During experimental tests, strain values were obtained by DIC.

In the numerical analysis, three constitutive models were evaluated: Ogden, Neo-Hookean and Mooney-Rivlin. Results obtained by each model were compared with experimental values to find out if there were any differences between them, invalidating the null hypothesis in the ANOVA statistical analysis.

2.1. Samples

In the analysis, four sample configurations were used (Fig. 2). The first one was a standard dumbbell-like, designed based on type B

samples of the BS 2782-2/EN ISO 527-2 standard, with a thickness of 4 mm (British Standard, 1996).

Samples' shape containing stress concentrators were based on the most common shapes evaluated when studying stress concentrations in metals. For this case, the thickness was 3 mm for all samples.

2.2. Experimental tests

2.2.1. Specimen preparation

Four aluminum molds were machined according to the shapes previously presented. The milling process was performed in a Deckel Maho DMC 63V CNC (computer numerical controlled) machine from the Mechanical Technology Laboratory of the Instituto Politécnico de Bragança (IPB).

After that, at IPB's Fluid Mechanics and Hydraulics Laboratory, PDMS was prepared and cast into the molds. To prepare the PDMS, prepolymer and curing agent were metered and mixed in a 10:1 mass ratio, respectively. The mixture was stirred manually in a Becker, using a spatula and then placed into a vacuum chamber to remove air bubbles. The PDMS used was the Sylgard 184.

Once filled, the molds were placed again in the vacuum chamber, to remove any remaining air bubbles. Thereafter, the specimens were cured for one week at room temperature (around $20°C$).

Cured samples were painted with a speckle pattern to ensure matching between images of the undeformed and deformed state. It should be mentioned that measurements by DIC depends on the quality of the speckle pattern, which can be the samples' surfaces natural texture or artificially made by spraying black or white paints (Pan et al., 2009).

In this study, three distinct speckle pattern arrangements were tested:

1st arrangement: A black pattern against a white background.
2nd A black pattern on a "natural" transparent background.
3rd A white speckle pattern on a black background.

Initially, a base sample (Standard BS 2782 sample) was subjected to all three arrangements and different painting methodologies. This approach allowed us to assess whether the stiffness of the dye layer, in relation to the test piece material, and the adhesion between the PDMS and the paint would affect the DIC analyses.

During this evaluation, different painting methodologies were tested, including specific rubber-sprays, general-purpose sprays, and general-purpose paints applied using an air compressor sprayer.
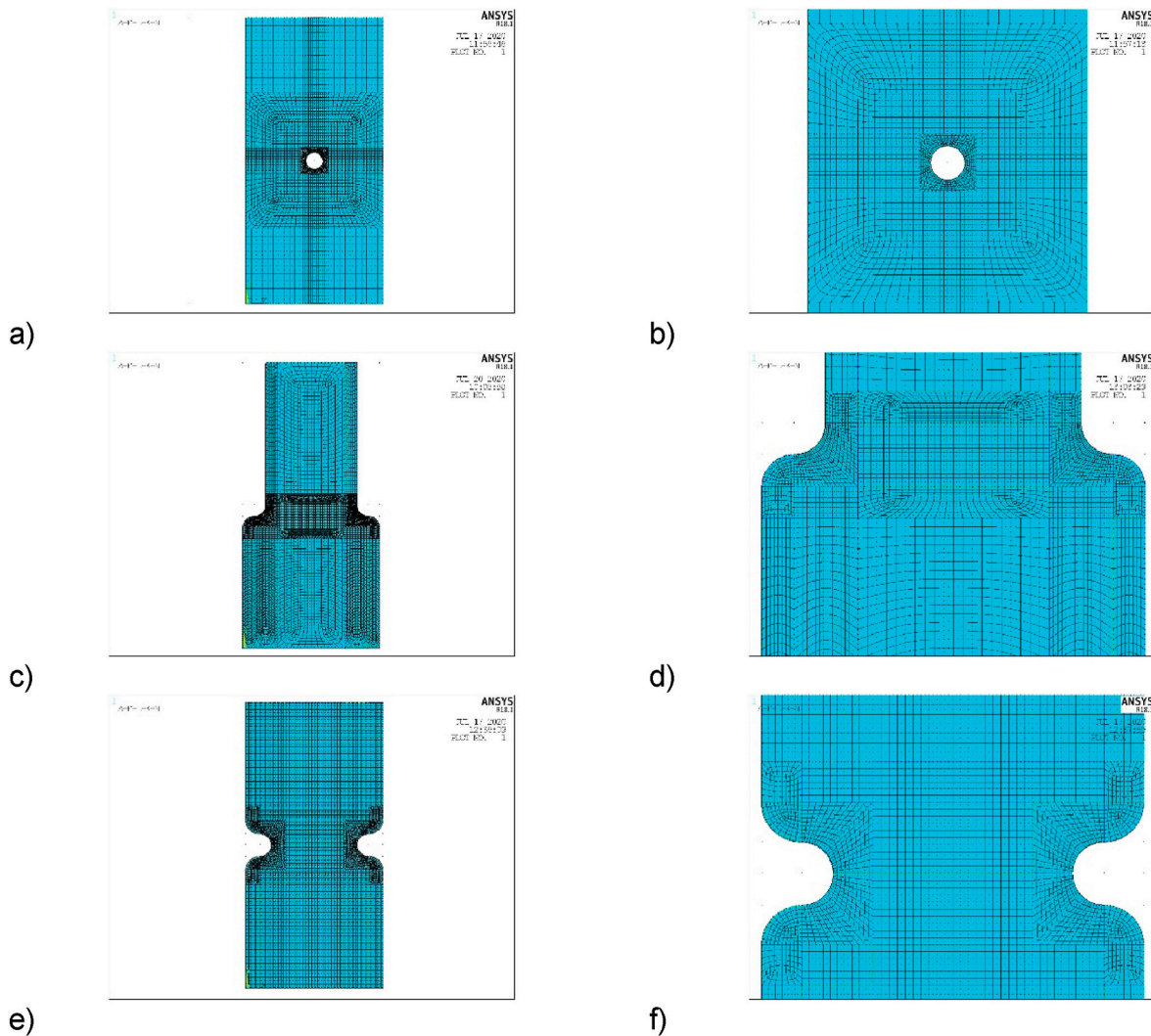
Fig. 5. Mesh created for the numerical simulations: Sample 1: a) overall view; b) zoomed at the higher resolution zone (center hole); Sample 2: c) overall view; d) zoomed at the higher resolution zone (shoulder fillet); Sample 3: a) overall view; b) zoomed at the higher resolution zone (edge node).

Table 1
Number of elements and nodes of the simulations.

Mesh Properties	Sample 1	Sample 2	Sample 3
Nodes	10240	16577	16533
Elements	3336	5434	5388

The evaluation process involved applying a tensile displacement at a rate of 5 mm/min, reaching a maximum strain of 20%. Following this, a visual assessment was performed to detect any signs of cracks or detachment of the paint layer from the specimen. Such detachment, leading to peel-off from the sample, could result in a loss of material deformation data (Zheng et al., 2020).

The testing revealed that the choice of paint and the painting process had a substantial impact on the success of the speckle pattern, transcending the arrangement of the pattern itself. Regardless the arrangement used, only the use of a spray suitable for rubber consistently delivered the required adhesion and capacity to accurately track the specimen's deformation.

Based on these findings and with the objective of ensuring consistent and accurate results across all samples, the speckle pattern arrangements were assigned as follows:

The first sample (with central holes) was painted with the first pattern arrangement (black against a white background) (Fig. 3a).

The second sample (shoulder-filleted geometry) utilized the second pattern arrangement (black on a "natural" transparent background) (Fig. 3b).

The third sample featured the third pattern arrangement (white on a black background) (Fig. 3c).

In all cases, the paint exhibited consistent ability to withstand substantial deformations without any peeling.

2.2.2. Tensile tests and DIC

Tensile tests were performed using a Shimadzu Autograph AGS-X 10 KN universal test machine, with manual wedge action tensile grips. The parameters for standard samples were defined according to BS 2782, with a test speed of 5 mm/min and the distance between grips as 120 mm.

Samples with stress concentration had a distance between grips of 60 mm and the test was set up to stop at a maximum engineering strain, 20%, which represented an upward 12 mm movement of the top grip. After waiting 10 s at this maximum value, both grips returned to the initial position and restart the process, during three cycles.

Images of the trials were acquired using a Canon EOS 7D, recording in 1080p HD resolution, resulting in images with dimensions of 1920x1088 pixels. The camera operated at a frame rate of 25 frames per second (fps) and proper supports and a lighting system, consisting of
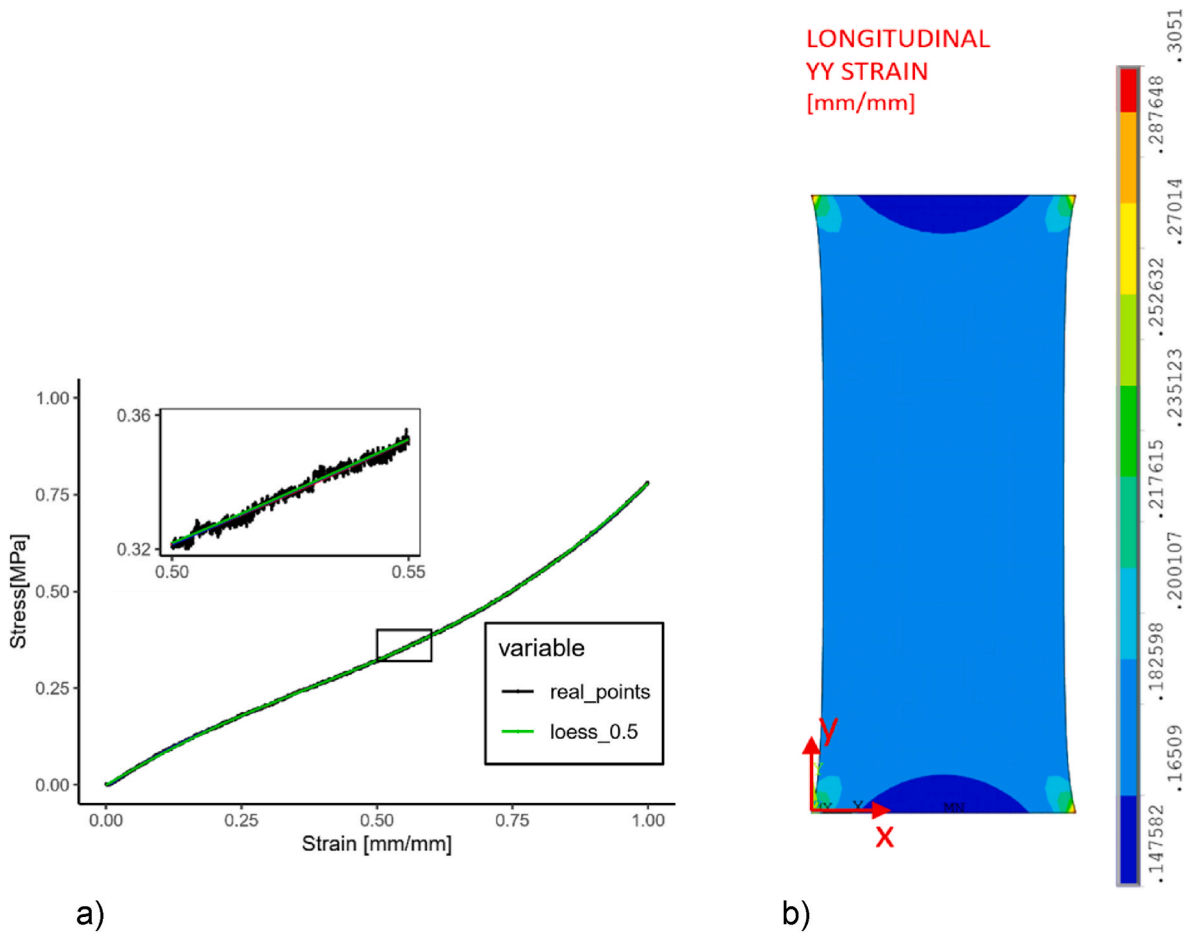
Fig. 6. Results from the standard reference sample: a) Stress-Strain curve for experimental results (Dark color) and data fitting (light color); b) Numerical Results for maximum strain.
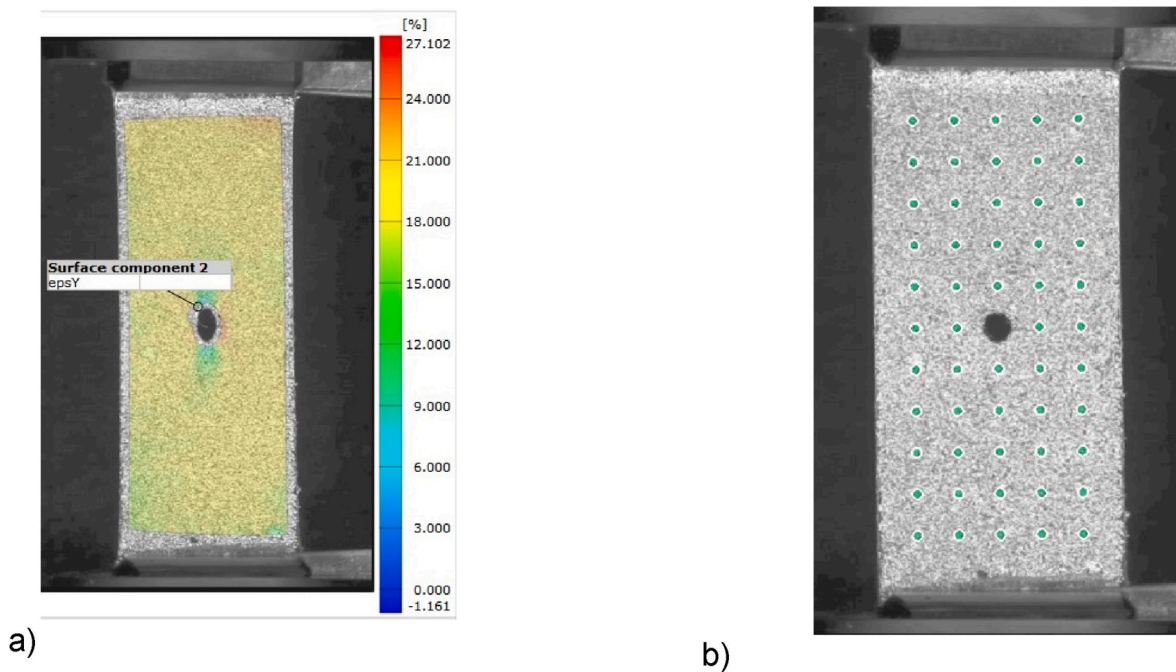

Fig. 7. Digital Image Correlation for the 1st Sample (with center hole): a) Longitudinal maximum strain recognized by the DIC software, showing higher strain values at the specimen's center strain values are given in %; b) Selected points for strain reading.
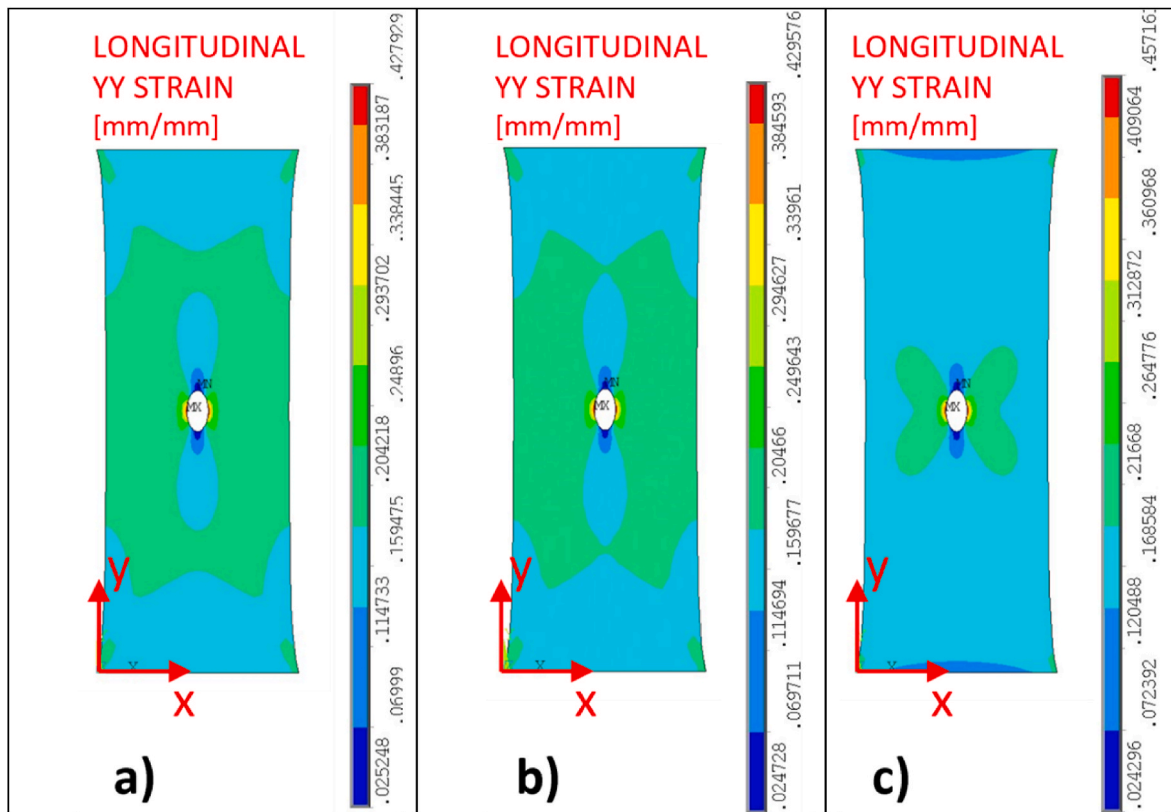
Fig. 8. Longitudinal ("YY") strain, at the maximum displacement step, obtained using numerical analysis of the 1st Sample (with center hole). Constitutive Models: a) Mooney-Rivlin; b) Ogden; c) Neo-Hookean.
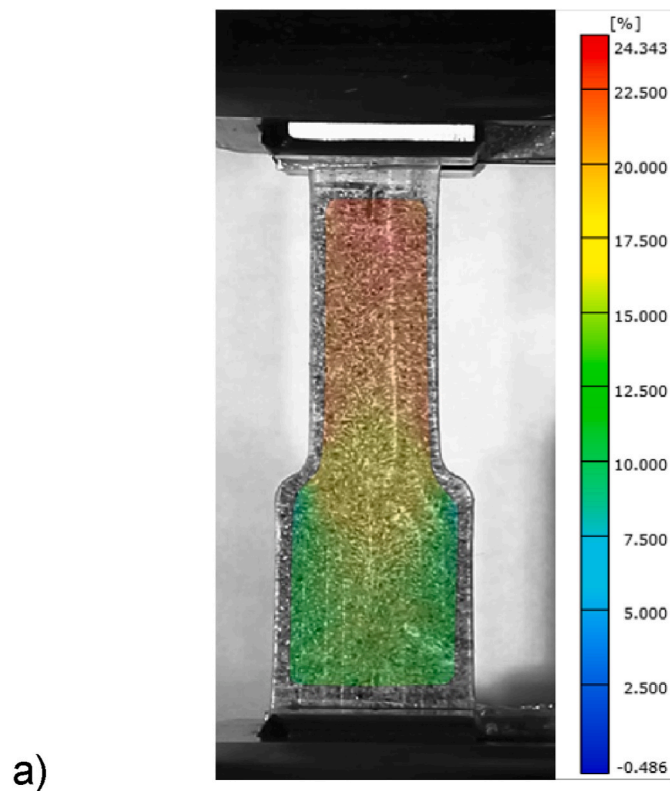

Fig. 9. Longitudinal ("YY") strain, at the maximum displacement step, obtained by the Digital Image Correlation for the 2nd Sample (with shoulder fillet)- strain values are given in %.

three 6W lamps, were provided. (Fig. 4). Each test had approximately 3000 frames, a massive amount of data to be processed by the DIC software. Therefore, a C++ routine was developed and used to reduce the total number of pictures by 90%, resulting in approximately 300 frames at regular intervals throughout the duration of the test, keeping track of the sample during the whole assessment.

The camera was positioned to capture longitudinal strain at the frontal face of the specimen, which presented the larger area of interest. Notably, there were no cameras monitoring changes in specimen thickness at the lateral sides, and therefore, transversal strains in those areas were not evaluated.

The DIC process was done using GOM® correlate software, with following parameters: facet size 19–23 pixels, point distance 16–19 pixels. Each dot within the speckle pattern ranged in diameter from 1.8x1.8 pixels to 5.7x5.7 pixels.

Inspection points for comparison were created manually and the total strain in the y direction of these points was measured.

2.3. Numerical analysis

In hyperelastic materials, the stress-strain relation derives from a Strain Energy Density function, also called Helmholtz Free-Energy Function, defined by constitutive models (Ψ) (Sasso et al., 2008).

2.3.1. Mooney-Rivlin model

This model can be derived from a hyperelastic model made of a polynomial series of $(I_1 - 3)$ and $(I_3 - 3)$ (Marckmann and Verron, 2006)– (Saccomandi and Vergori, 2019), as shown in Equation (1):

$$\Psi = \sum_{i=0}^{\infty} \sum_{j=0}^{\infty} C_{ij}(I_1 - 3)^i (I_2 - 3)^j \qquad (1)$$
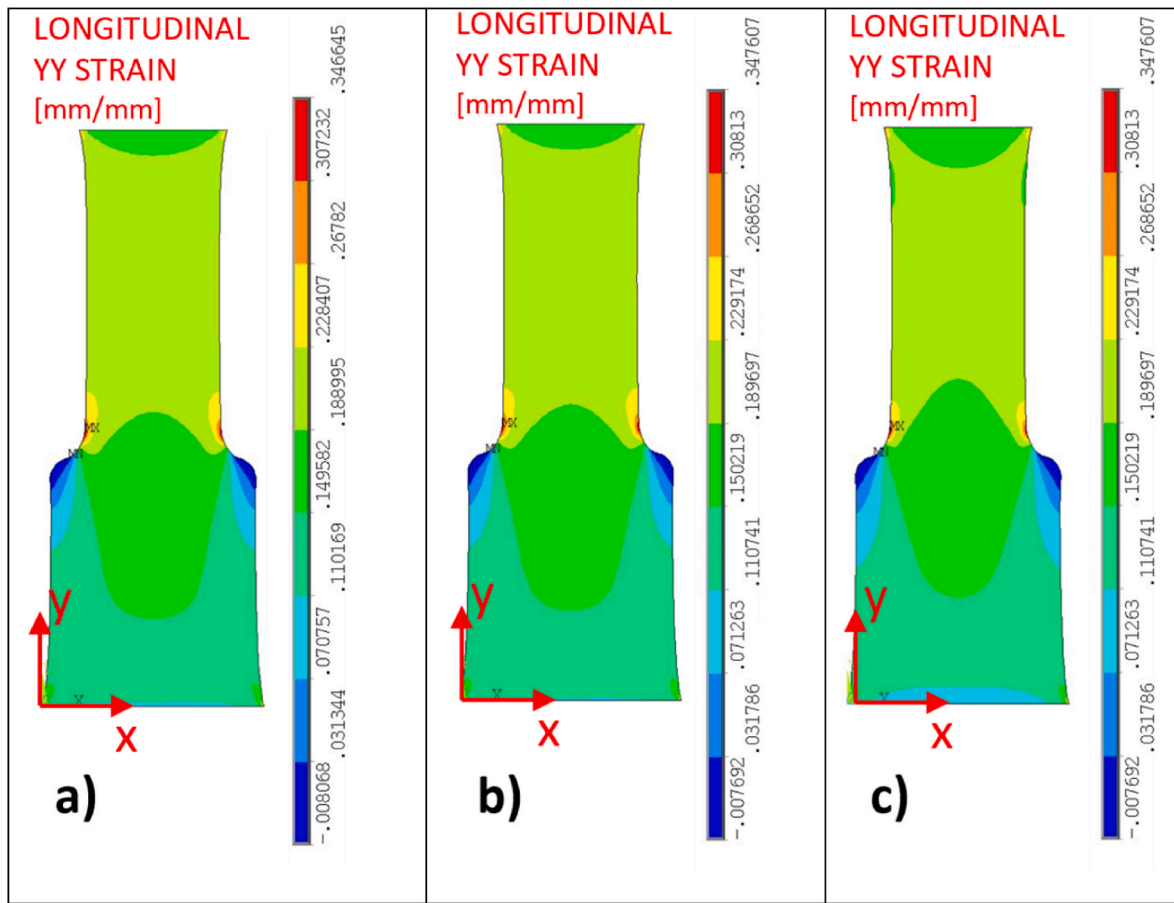
Where:

Fig. 10. Longitudinal ("YY") strain, at the maximum displacement step, obtained by the numerical analysis of the 2nd Sample (with shoulder fillet): Constitutive Models: a) Mooney-Rivlin; b) Ogden; c) Neo-Hookean.

$$C_{00} = 0; \tag{2}$$

$$C_{10} + C_{01} = v; \tag{3}$$

$$\sum_{i+j=n}^{\infty} C_{ij} = 0 \forall n \in N - 1 \tag{4}$$

being: v the infinitesimal shear modulus, constants defined by the stress-strain curve of the material. The condition on (2) imposes null energy in the reference position, while (3) guarantees a relationship with the linear elasticity theory, and (4) allows linear relationships between torque, shear stress and shear strain, and in the amount of twist in simple shear and torsion, respectively (Saccomandi and Vergori, 2019).

2.3.2. Neo Hookean model

Consider the variation of Ψ only in function of I_1 invariant, as shown in Equation (5).

$$\Psi = C_1(I_1 - 3) \tag{5}$$

2.3.3. Ogden Model

Ogden (1972b) proposed that the strain-energy function can be written by the following equation:

$$\Psi = \sum_{i=1}^{\infty} \mu_i \varphi(\alpha_i) \tag{6}$$

Where:

$$\varphi(\alpha_i) = \left(\lambda_1^{\alpha_i} + \lambda_2^{\alpha_i} + \lambda_3^{\alpha_i} - 3 \right) / \alpha_i \tag{7}$$

μ_i and α_i are determined by the stress-strain curve of the material, just like the Mooney-Rivlin model. Lambdas (λ) are the principal stretches in the three directions (x, y, and z). Ogden (1972b) showed that for uniaxial tensions, a two-term strain-energy function produces very satisfactory results when it is compared with experimental data.

2.3.4. Numerical simulation

Each one of the three different samples were simulated numerically in ANSYS Mechanical APDL using the constitutive models previously presented (1-parameter Ogden, Neo-Hookean, Mooney-Rivlin 3-parameters) and data from the standard sample stress-strain curve. For all the tests, only the region between grips was designed in the software. To simulate, PLANE183 with 8 nodes was chosen as the element type. For this element, all information is inside the constitutive model. So, once the model's constants were calculated, there was no need to specify any other material property in the model.

Regarding the mesh sensitivity analysis, a three-phase approach was adopted to ensure mesh convergence. This approach involved delineating distinct regions within the mesh and implementing variable element sizes, with particular emphasis on maintaining smaller elements at locations of the stress raisers or where higher strain values were forecasted, notably in the vicinity of the center hole and fillets.

The convergence test entailed the iterative adjustment of element sizes until the disparity between the current and previous steps, concerning the maximum strain in the "yy direction", fell below the 2% threshold. In the initial test phase, the largest elements measured 4 mm, while the smallest reached 0.5 mm. Subsequently, during the subsequent testing phase, elements ranging from 0.25 mm to 2 mm were used, resulting in variations ranging from 1.8% to 3% compared to previous
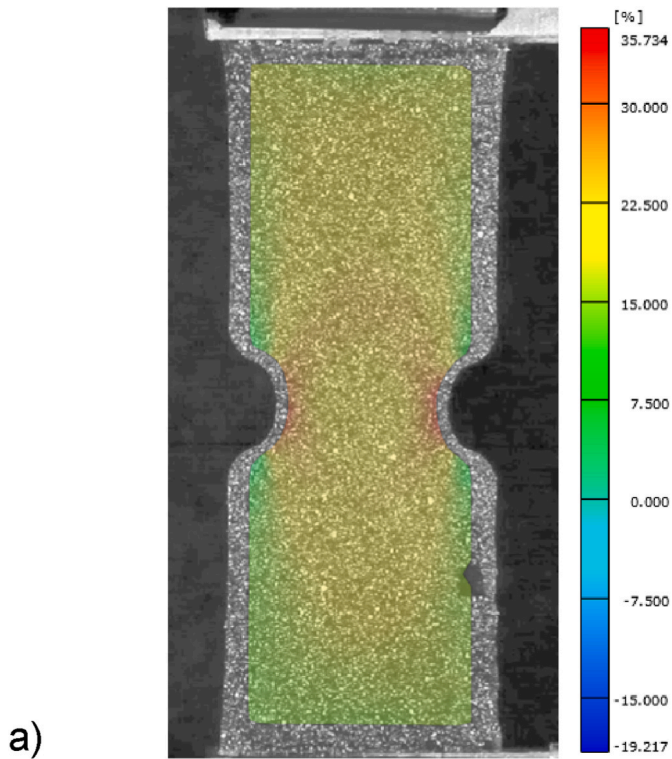
Fig. 11. Longitudinal ("YY") strain, at the maximum displacement step, obtained by the digital Image Correlation for the 3rd sample (with edge notches)-strain values are given in %.

results. This led to a further reduction in element sizes during the final iteration, resulting in dimensions spanning from 0.125 mm to 1 mm. In this phase, the discrepancy relative to the previous iteration ranged from approximately 0.8%–2%. As considerable computational overhead was encountered and the mesh contained a substantial number of elements, ranging from 3336 to 5434, pursuing further reductions in element size became progressively less practical and efficient. Consequently, this phase of the study was concluded.

The final mesh (Fig. 5) shows smooth changes between mesh regions and a number of nodes and elements for each specimen as shown in Table 1.

The boundary conditions were applied considering that nodes on the bottom did not have any movement on "*y axis*" and top nodes had a longitudinal displacement of 12 mm on "*y*" (20% of the total height). Both nodes did not have any transversal displacement (on "*x*"). The entire simulation was calculated using 5000 sub steps, considering as maximum 10000 sub steps and minimum as 1000 sub steps.

To compare results with DIC data, it was necessary to export the node's coordinates, the elements' nodes, and the nodes and elements' longitudinal strain.

2.3.5. Stress concentration factor

The Stress Concentration Factor (K) is a ratio between the highest stress that can be supported by an element with a discontinuity and the nominal stress in an element without stress concentrator, but with same loading condition (Pilkey, 2020). There are a lot of discontinuities, each one with its particular K, which could be, for instance, a center hole, an edge notches or shoulder fillets. It is a theoretical factor, derived from the theory of elasticity or from experimental tests (Pilkey, 2020).
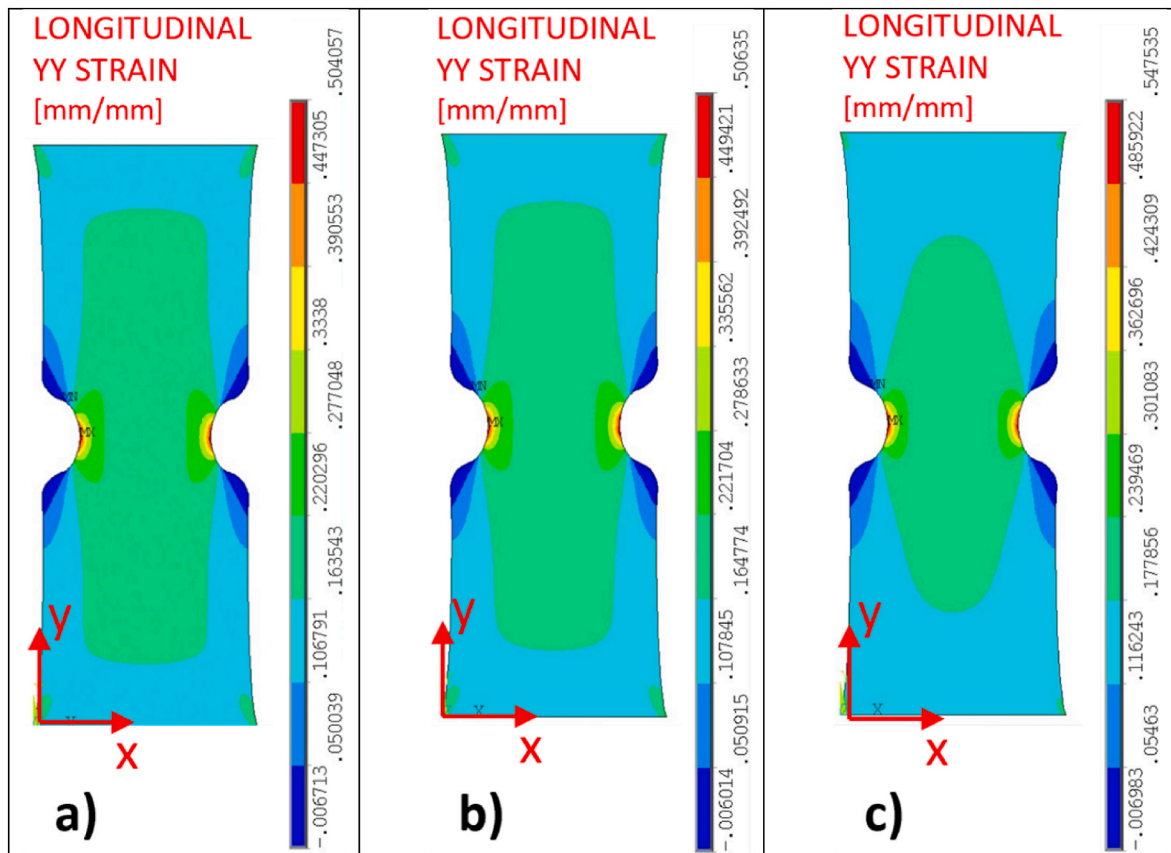
Fig. 12. Longitudinal ("YY") strain, at the maximum displacement step, for the longitudinal YY strain, obtained by the numerical analysis of the 3rd Sample (with edge notches). Constitutive Models: a) Mooney-Rivlin; b) Ogden; c) Neo-Hookean.
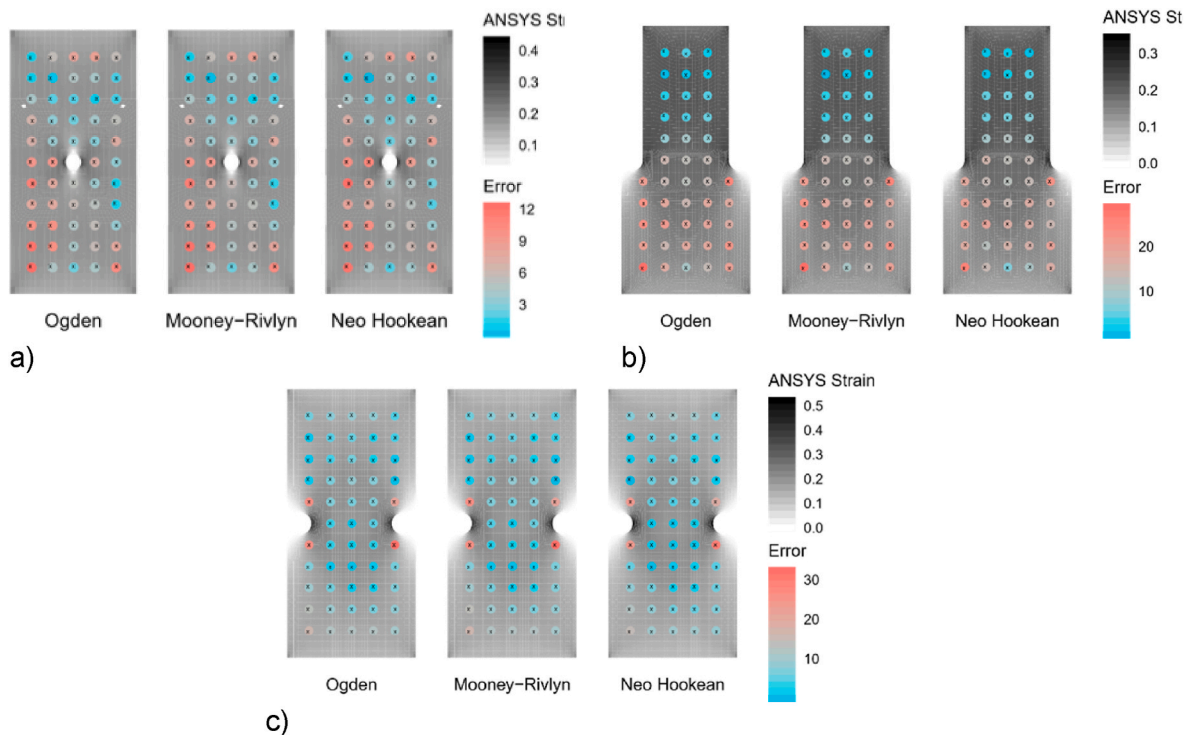
Fig. 13. Comparison between numerical simulation and DIC test results. A respective error is shown at each DIC data point, lighter blue colors represent smaller errors, while darker red color represent higher errors. The error scale is in %. Comparisons are presented for: a) 1st sample; b) 2nd sample; c) 3rd sample.

3. Results

The digital image correlation software was able to obtain many points, creating strain vs time curves for each of these points.

After, the strain at each point was compared with the strain presented by numerical simulations.

3.1. Reference sample

The Hyperelastic Models need specific constants for the correct curve definition. These constants are obtained through stress-strain experimental curve from reference sample. This curve is represented by a darker line in Fig. 6a.

However, there are regions (zoomed in Fig. 6a) with slight data variations that can disturb the simulation behavior on the numerical analysis. So, a curve adjustment using loess (local weighted regression) method was done. For this test, three different span parameters were chosen: 10%, 25% and 50%. As all of them showed good approximation for the tested points (lines overlapped), it was chosen the 50% loess model, in a lighter color (green) in Fig. 6a.

The simulation without stress raisers revealed constant stress and strain values in the specimen's middle area. As shown in Fig. 6b, only areas near the fixation and at the specimen's border, had higher strain values. The same pattern is expected in experimental tests, as the grips can compel stresses in the sample during the experiment.

3.2. 1st sample

Due to the hole's presence highest contrast in the strain gradient, shown in Fig. 7 for the 1st sample, was obtained at specimen's central points, mainly in the load application axis. Discrete values were obtained at selected points all over the specimen (Fig. 7b).

The longitudinal, strain contour obtained at the step with maximum displacement of the numerical analysis, presented high similarity with the strain from experimental results, as shown in Fig. 8. Also, the

contour has higher similarity with Mooney-Rivlin and Ogden's constitutive models. The Neo-Hookean presented a region with higher intermediate strain in the center, in a butterfly-like shape. This scattering pattern usually occurs in intermediary stages of elastomers elongation, as an orientation is defined along the stretching direction (Hu et al., 2019).

3.3. 2nd sample

Due to a reduction in the cross-sectional area next to the fillets, the specimen's upper region received higher stresses and, consequently, underwent bigger strains. The DIC showed a gradient of deformation values, ranging from the least deformed base, with values around 10%, to the most deformed top, with almost 25% strain (Fig. 9).

The three models showed similar contour plots (see Fig. 10). However, unlike the strain gradient obtained by DIC, in the numerical analysis regions of the shoulder fillets showed highest values, emphasizing this geometry emphasizing the way in which it acts as a stress raiser.

3.4. 3rd sample

Besides having a higher strain value in the center area, due to smaller cross-section, the strain shape contour on both: simulation (Fig. 12) and the DIC test (Fig. 11) seemed similar, which by itself showed some correspondence between tests and simulations.

3.5. Comparison between the numerical constitutive models and statistical analysis

Fig. 13 shows the longitudinal strain, at the maximum displacement step, for each element in the simulation (in a grayscale), the selected points' error (as a blue-red scale), compared with each numerical simulation, and the nearest point position (as an "x") for both comparison methods.
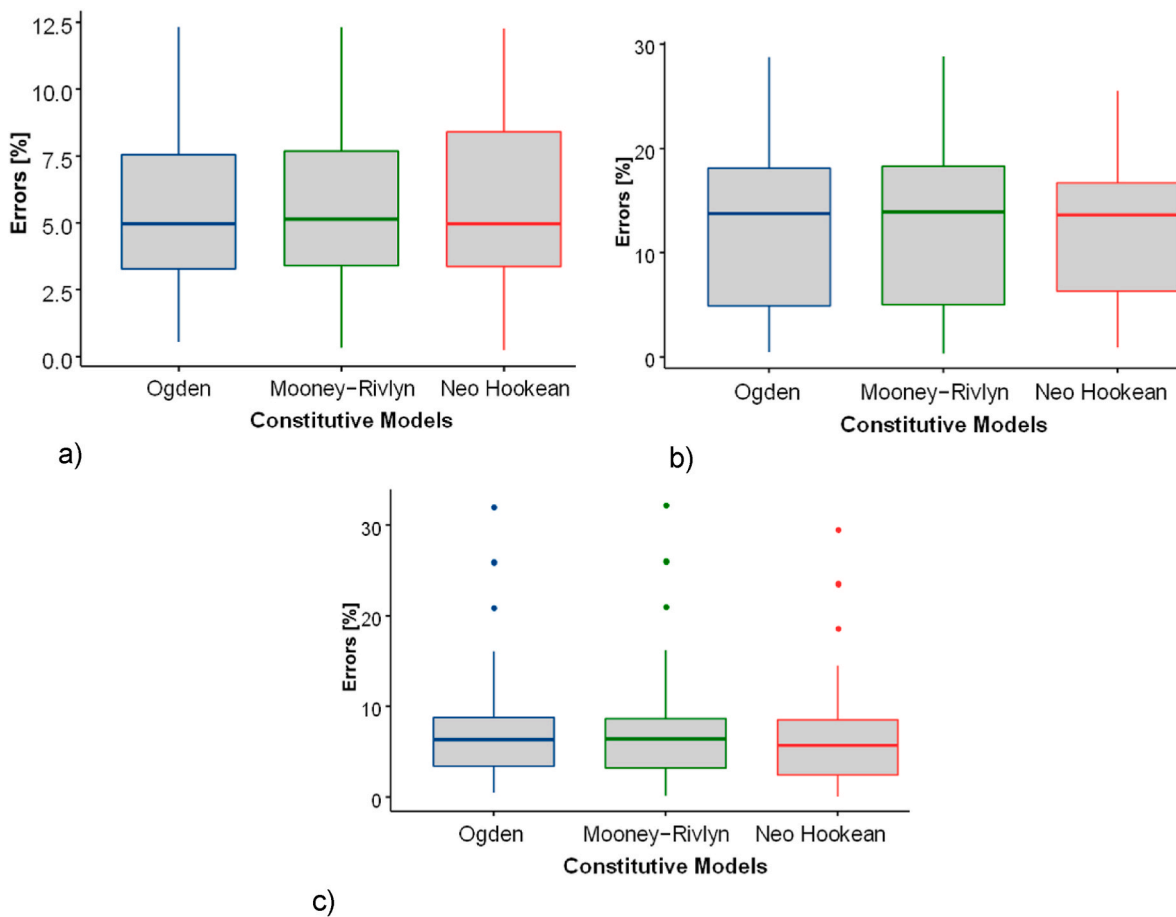
Fig. 14. Box plot of the errors presented by each constitutive model for the samples: a) 1st sample, showing no outliers and smaller errors among the models analyzed; b) 2nd sample, with the biggest interquartile range among the 3 models; c) 3rd sample, with some outliers.

Table 2
Results of the ANOVA for each sample.

Sample	Analysis	DOF	SS	MS	F	P
1st	Variable	2	1,948	0,974	0,1026	0,9025
	Residuals	159	1508,829	9,489		
2nd	Variable	2	25,042	12,521	0,2476	0,7811
	Residuals	126	6373,005	50,579		
3rd	Variable	2	16,585	8,292	0,1999	0,8190
	Residuals	156	6471,766	41,486		

DOF= The degrees of freedom, SS= the sum of squares, MS= the mean sum of squares, F= the F-statistic, P= the P-value.

For the 1st and 2nd samples (Fig. 13a) all the constitutive models showed higher error distribution on the samples' bottom-left region, which can indicate some deviation in the DIC evaluation, due to the difficulty to fix specimens on the experimental apparatus, these errors are results from the out-of-plane displacement, one of the main error causes in image correlations (Haddadi and Belhabib, 2008). Although small-thickness specimens typically demonstrate reduced susceptibility to out-of-plane displacement, it is essential to consider that, as we reached 20% strain in the "yy direction" and given the material's high Poisson ratio, which may reach up to 0.5 (Cho et al., 2021), the reduction in thickness from the original 4 mm may introduce the possibility of out-of-plane errors. For 3rd sample, the biggest errors were observed in the central region, close to edge notches. At all other points, errors were low and equally distributed. This is a consequence of the speckle pattern and the DIC process. The difficulty of ensuring that all ink dots maintain good adherence in areas with high strain, in addition to missing pixels in the image and correlation algorithm, creates areas where higher errors are expected. Considering the errors on all the samples, as the material is exceptional flexibility and manual wedge action tensile testing grips were used, achieving impeccable specimen alignment during positioning can indeed be a challenging endeavor. This less-than-ideal alignment may lead to the introduction of additional deformation modes beyond pure axial tension, consequently giving rise to complex stress distributions within the material and potentially introducing errors.

The box plots, in Fig. 14, show that the error distribution of all constitutive models is similar and around 5% for the 1st sample, 14% for the 2nd and 7% for the 3rd.

The ANOVA tests (Table 2) prove that, for all samples, there is not any significant difference between the constitutive models, as the F-values are smaller than P-values, validating the null hypothesis.

The Tukey HSD plot (Fig. 15) shows a visual approach to the comparison. The P-value was above 0.05 (5% confidence interval), which means there are no significant differences between the constitutive models O, M, and N (Ogden, Mooney-Rivlin and Neo Hookean models, respectively). As all the lines of the comparison intervals (dashed vertical line), cross the zero point, there are no significant difference between these elements.

3.6. Evaluation of the stress concentration factors

To assess the stress concentrators, it was necessary to compare the stress from the central cross-section of each sample (Fig. 16). The reference sample presented an almost constant stresses in its center. These stresses are the reference used for calculating the stress
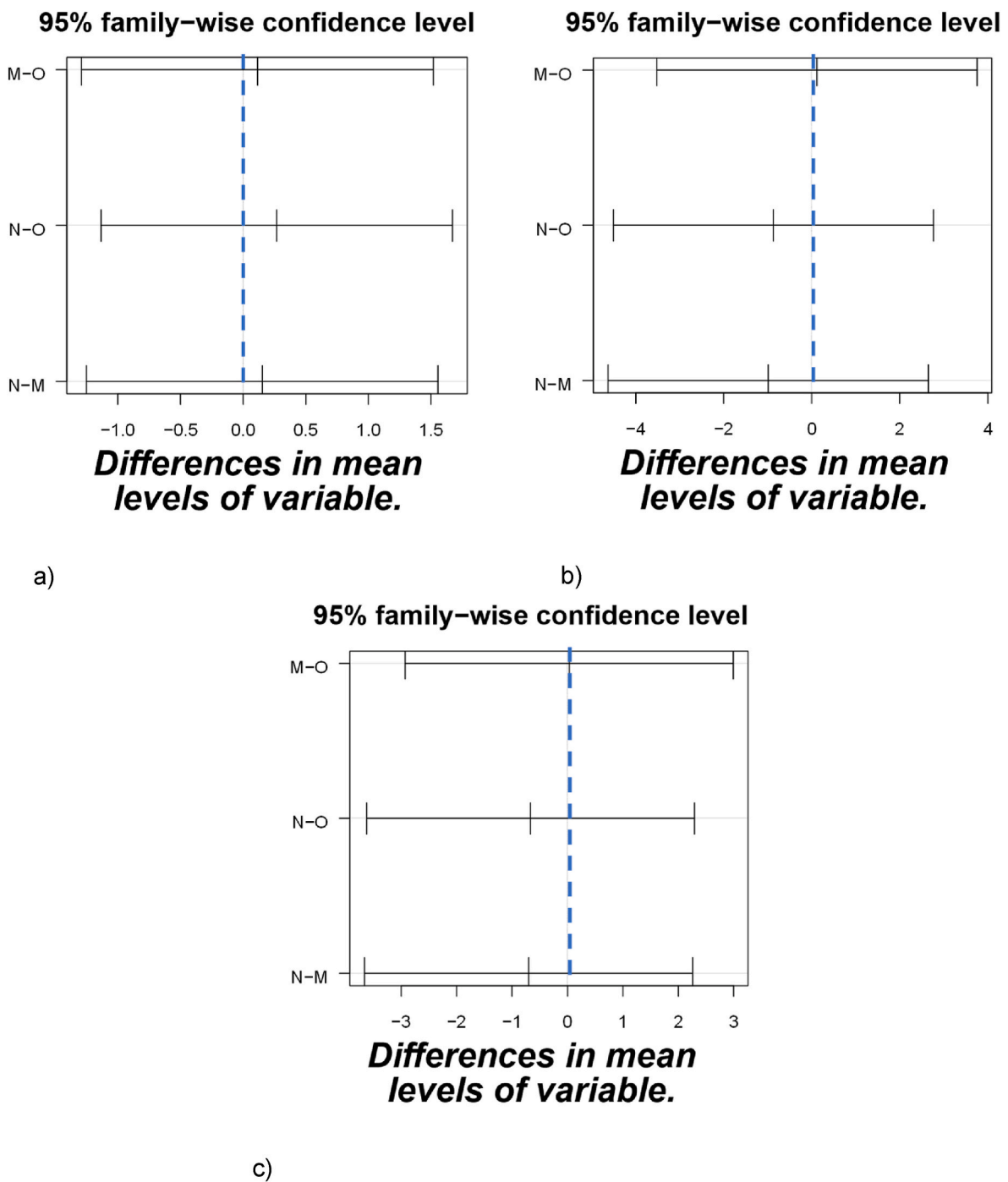
a)

b)

c)

Fig. 15. Tukey plot of the ANOVA analysis, for the samples: a) 1st sample; b) 2nd sample; c) 3rd sample.

concentration factor.

As the ANOVA proved there is no difference between the constitutive models, calculation of the stress concentration factors was performed only for the Ogden model. For this model, the stress distribution in the center of each sample is shown in Fig. 8.

The stress concentration factors obtained are shown in Table 3. The symmetric semicircular edge notches specimen has the highest value, a consequence of it having the lowest cross-section area.

The specimen with a central hole has a K value of 2.051, which is 30% smaller than those presented for a generic neo-Hookean material with a center hole, found in the literature (Jiang et al., 2023). This represents a validation for the data of this study, as differences of this order can be the result of punctual differences between materials. Also,

JIANG e colab., 2023, values approach of 2 as the central hole becomes more elliptical. Because the characterized PDMS had great stretch-ability, as the test proceeds, the hole tends to quickly assume an elliptical shape.

4. Conclusion

Firstly, was addressed a comparison between three different constitutive models for hyperplastic materials: Ogden, Mooney-Rivlin, and Neo Hookean. The ANOVA results and Tukey plots showed that there is no significant difference between the constitutive models, which implies that for the numerical analysis of PDMS, any model can be chosen. Also, the strain pattern, depict by the numerical analysis for each of these
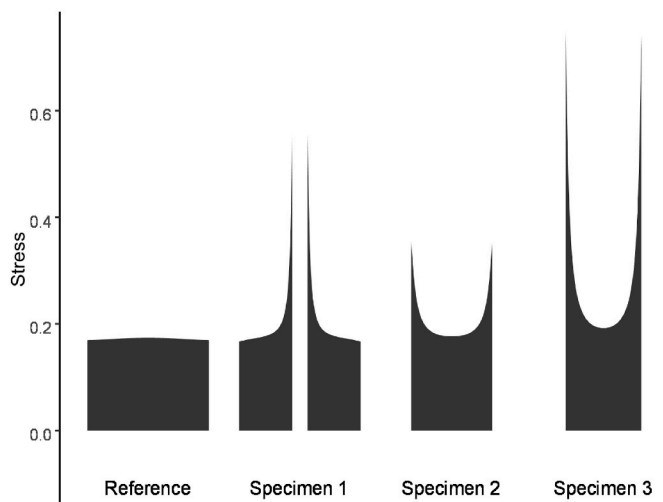
Fig. 16. Numerical Stresses at the central cross section of each sample.

Table 3
Stress concentration factor (K) for each sample.

Sample	Stress Concentration Factor
1st	3.229
2nd	2.051
3rd	4.323

models, resembles the pattern assessed by Digital Image Correlation, which implies there is a huge equivalence of results obtained by the simulation with the real samples behavior obtained in the experimental tests.

When comparing experimental results with the numerical ones, the error had similar behavior for each constitutive model. However, given the absence of experimental data in the vicinity of the stress concentrators and the likelihood of higher errors in these areas, a more meticulous analysis of these regions may reveal that these discrepancies could be attributed to specific variations between the chosen constitutive law and the experimental data. This in-depth analysis has the potential to discern distinct behaviors for different models.

When analyzing the discrete values, higher errors were found on the same regions over the specimens. This behavior indicates that the deviations occurred as results of errors during the image capture process. The highest error values were obtained in the 2nd sample, due to issues caused by specimen fixation into the machine, as the soft material does not present high resistance against clamp system. In addition, out-of-plane displacement and speckle pattern generation are characteristics to be concerned about when analyzing Digital Image Correlations.

In summary, this study did not find a preferable constitutive model to analyze the material and to evaluate the stress concentrator factor itself. This way, only the Ogden model was used to evaluate this constant. The value for a with a central hole sample was 2.051, near that presented in the literature. For the remaining geometries, there was no other study that previously assessed the factor for shoulder-filleted or edge-node samples. Thus, new values were defined for variables needed during the analysis of hyperelastic materials. Such collaboration is significant, considering the growth of studies and the usage of these materials. More broadly, our approach provides a foundation for understanding the PDMS stress-strain behavior.

As the three sample shapes selected (with a central hole, shoulder-filleted, and edge-node) are among the most studied geometries, and with well-known K value curves for other materials, such as metals. These are important shapes for engineers and designers when applying empirical or numerical knowledge to develop new parts and structures.

Further experiments are needed to create K-curves, K-equations or simply acquire more data about the stress effect in other geometries, for instance, in elliptical holes or distinct relations between the larger and the smaller cross-section in a specimen with shoulder fillets. Furthermore, data refinement is needed specifically around the stress concentration geometries. Future research endeavors may explore alternative speckle patterns, such as those created using airbrushes, to achieve more consistent spot sizes and improved surface coverage on the test piece.

CRediT authorship contribution statement

Flaminio Cesar Sales: Writing – original draft, Visualization, Validation, Software, Formal analysis, Data curation. **Andrews Souza:** Writing – original draft, Visualization, Validation, Investigation. **Fallconny R.S. Oliveira:** Writing – original draft, Visualization, Software, Formal analysis. **Rui A. Lima:** Writing – review & editing, Resources, Methodology, Investigation. **João Ribeiro:** Writing – review & editing, Supervision, Resources, Project administration, Methodology, Investigation, Formal analysis, Conceptualization.

Declaration of competing interest

The authors of this manuscript declare that they have not any conflict of interests.

Data availability

No data was used for the research described in the article.

References

An, A.K., et al., 2017. PDMS/PVDF hybrid electrospun membrane with superhydrophobic property and drop impact dynamics for dyeing wastewater treatment using membrane distillation. J. Membr. Sci. 525, 57–67. October 2016.

Ariati, R., Sales, F., Souza, A., Lima, R.A., Ribeiro, J., 2021. Polydimethylsiloxane composites characterization and its applications: a review. Polymers 13 (23), 4258.

British Standard, 1996. BS EN ISO 527-2/BS 2782-3: Method 322: Plastics — Determination of Tensile Properties. London.

Chang, J.H., Li, J.E., 2010. Evaluation of the energy change due to presence of multiple irregularly shaped inclusions in hyperelastic solids. Finite Elem. Anal. Des. 46 (4), 339–347.

Cho, H.S., Kim, H.A., Seo, D.W., Jeoung, S.C., 2021. Poisson's ratio measurement through engraving the grid pattern inside poly(dimethylsiloxane) by ultrafast laser. Jpn. J. Appl. Phys. 60 (10), 101004.

Dwivedi, K.K., Lakhani, P., Kumar, S., Kumar, N., 2022. A hyperelastic model to capture the mechanical behaviour and histological aspects of the soft tissues. J. Mech. Behav. Biomed. Mater. 126, 105013.

Fukahori, Y., Seki, W., 1993. Stress analysis of elastomeric materials at large extensions using the finite element method. J. Mater. Sci. 28 (15), 4143–4152.

Haddadi, H., Belhabib, S., 2008. Use of rigid-body motion for the investigation and estimation of the measurement errors related to digital image correlation technique. Opt Laser. Eng. 46 (2), 185–196.

Hu, H., et al., 2019. Biodegradable elastomer from 2,5-Furandicarboxylic acid and ε-caprolactone: effect of crystallization on elasticity. ACS Sustain. Chem. Eng. 7 (21), 17778–17788.

Jiang, Y., Li, D., Chen, Y., Huo, Y., 2023. Analysis of stress and strain concentration around a centralized elliptical hole in a monodomain liquid crystal elastomer sheet. Int. J. Solid Struct. 264, 112079.

Khajehsaeid, H., Reese, S., Arghavani, J., Naghdabadi, R., 2016. Strain and stress concentrations in elastomers at finite deformations: effects of strain-induced crystallization, filler reinforcement, and deformation rate. Acta Mech. 227 (7), 1969–1982.

Khaniki, H.B., Ghayesh, M.H., Chin, R., Amabili, M., 2023. Hyperelastic structures: a review on the mechanics and biomechanics. Int. J. Non Lin. Mech. 148, 104275.

Kim, B., et al., 2012. A comparison among Neo-Hookean model, Mooney-Rivlin model, and Ogden model for chloroprene rubber. Int. J. Precis. Eng. Manuf. 13 (5), 759–764.

Marckmann, G., Verron, E., 2006. Comparison of hyperelastic models for rubber-like materials. Rubber Chem. Technol. 79 (5), 835–858.

Miranda, I., et al., 2021. Properties and applications of PDMS for biomedical engineering: a review. J. Funct. Biomater. 13 (1), 2.

Montazerian, H., et al., 2019. Permeability and mechanical properties of gradient porous PDMS scaffolds fabricated by 3D-printed sacrificial templates designed with minimal surfaces. Acta Biomater. 96, 149–160.

Myneni, M., Benjamin, C.C., Rajagopal, K.R., 2021. Stress concentration factors around a circular hole in two fiber reinforced materials under large deformations. Mech. Mater. 163, 104089.

Nunes, L.C.S., 2011a. Mechanical characterization of polytetrafluoroethylene polymer using full-field displacement method. Opt Laser. Eng. 49 (5), 640–646.

Nunes, L.C.S., 2011b. Mechanical characterization of hyperelastic polydimethylsiloxane by simple shear test. Mater. Sci. Eng. A 528 (3), 1799–1804.

Ogden, R.W., 1972a. Large deformation isotropic elasticity – on the correlation of theory and experiment for incompressible rubberlike solids. Proc. R. Soc. London. A. Math. Phys. Sci. 326 (1567), 565–584.

Ogden, R., 1972b. Large deformation isotropic elasticity – on the correlation of theory and experiment for incompressible rubberlike solids. Proc. R. Soc. London. A. Math. Phys. Sci. 326 (1567), 565–584.

Pan, B., Qian, K., Xie, H., Asundi, A., 2009. Two-dimensional digital image correlation for in-plane displacement and strain measurement: a review. Meas. Sci. Technol. 20 (6), 062001.

Pereira, A.L., Banea, M.D., Neto, J.S.S., Cavalcanti, D.K.K., 2020. Mechanical and thermal characterization of natural intralaminar hybrid composites based on sisal. Polymers 12 (4), 866.

Pilkey, D.P.W., 2020. PETERSON'S STRESS CONCENTRATION FACTORS, fourth ed. Wiley.

Ribeiro, J.E., Lopes, H., Martins, P., Braz-César, M., 2019. Mechanical analysis of PDMS material using biaxial test. AIMS Mater. Sci. 6 (1), 97–110.

Rivlin, R.S., 1948. Large elastic deformations of isotropic materials IV. further developments of the general theory. Philos. Trans. R. Soc. London. Ser. A, Math. Phys. Sci. 241 (835), 379–397.

Rodrigues, R.O., Pinho, D., Bento, D., Lima, R., Ribeiro, J., 2016. Wall expansion assessment of an intracranial aneurysm model by a 3D Digital Image Correlation System. Measurement 88, 262–270.

Russ, J., Slesarenko, V., Rudykh, S., Waisman, H., 2020. Rupture of 3D-printed hyperelastic composites: experiments and phase field fracture modeling. J. Mech. Phys. Solids 140, 103941.

Saccomandi, G., Vergori, L., 2019. Generalised Mooney–Rivlin models for brain tissue: a theoretical perspective. Int. J. Non Lin. Mech. 109, 9–14.

Sales, F., et al., 2021. Composite material of PDMS with interchangeable transmittance: study of optical, mechanical properties and wettability. J. Compos. Sci. 5 (4), 110.

Sales, F.C.P., Ariati, R.M., Noronha, V.T., da Costa, R.R.C., Ribeiro, J.E., 2022. PU tensile tests: conventional and digital image correlation analysis. Procedia Struct. Integr. 37, 389–396.

Sasso, M., Palmieri, G., Chiappini, G., Amodio, D., 2008. Characterization of hyperelastic rubber-like materials by biaxial and uniaxial stretching tests based on optical methods. Polym. Test. 27 (8), 995–1004.

Shi, Y., Hu, M., Xing, Y., Li, Y., 2020. Temperature-dependent thermal and mechanical properties of flexible functional PDMS/paraffin composites. Mater. Des. 185.

Song, K., Cho, N.-K., Park, K., Kim, C.-S., 2022. Investigating mechanical behaviours of PDMS films under cyclic loading. Polymers 14 (12), 2373.

Souza, A., Marques, E., Balsa, C., Ribeiro, J., 2020. Characterization of shear strain on PDMS: numerical and experimental approaches. Appl. Sci. 10 (9).

Wang, F., Lei, S., Ou, J., Li, W., 2019. Effect of PDMS on the waterproofing performance and corrosion resistance of cement mortar. Appl. Surf. Sci. 507, 2020.

Wolf, M.P., Salieb-Beugelaar, G.B., Hunziker, P., 2018. PDMS with designer functionalities—properties, modifications strategies, and applications. Prog. Polym. Sci. 83, 97–134.

Yang, Z., Kim, C.-B., Cho, C., Beom, H.G., 2008. The concentration of stress and strain in finite thickness elastic plate containing a circular hole. Int. J. Solid Struct. 45 (3–4), 713–731.

Zheng, Q., Mashiwa, N., Furushima, T., 2020. Evaluation of large plastic deformation for metals by a non-contacting technique using digital image correlation with laser speckles. Mater. Des. 191, 108626.

Zhou, H., Su, Y., Chen, X., Yi, S., Wan, Y., 2010. Modification of silicalite-1 by vinyltrimethoxysilane (VTMS) and preparation of silicalite-1 filled polydimethylsiloxane (PDMS) hybrid pervaporation membranes. Sep. Purif. Technol. 75 (3), 286–294.